# Analysis of Morphology and Elemental Composition of (Ti-Zr-Hf-V-Nb)N High-entropy Alloys

A.A. Bagdasaryan, M.O. Bilokur*

*Sumy State University, 2, Rimsky-Korsakov Str., 40007 Sumy, Ukraine*

(Ti-Hf-V-Nb-Zr)N nanocomposite coating obtained by vacuum arc deposition method was investigated. Such techniques as Rutherford backscattering spectrometry (RBS), Secondary ion mass spectrometry (SIMS) and Glow Discharge Mass Spectrometry (GDMS) were used to conduct analysis of the structure of the coating, elemental distribution and composition of the elements.

**Keywords:** High-entropy alloy, Nitride coating, Depth profiles, Elemental composition, Ion beam technique.

PACS numbers: 81.05.Je, 81.70.Jb

## 1. INTRODUCTION

Recently, Yeh et al. developed a new class of metal compounds; so-called high-entropy alloys [11-16]. The concept of such alloys assumes at least 5 principal elements and the formation of the stable single-phase solid solution. The high entropy of mixing can stabilize the formation of a single-phase solid solution and prevent the formation of intermetallic compound during solidification. These alloys can possess various outstanding properties such as high hardness along with good ductility and durability, good wear resistance, good corrosion resistance and etc [17-22]. The nitride coatings of the high-entropy alloys are often used as the diffusion barriers in interconnects due to presumably high diffusion resistance [22-25].

In addition, the serious lattice distortions caused by the different sizes of atoms of the constituent elements decrease the coefficient of diffusion of the atoms, thereby reducing the growth of crystallites. Therefore, as it was previously shown from [26, 27], high-entropy alloys tend to form nanosize structures. As it is known from [28-34], the size reduction down to nanometer scale leads to significant changes in physical and mechanical properties. In turn, the structure and state of the grain boundaries are also important in the nanocrystalline materials. Thus, the preparation of new materials of nanocomposite coatings of the (Ti-Hf-Zr-V-Nb)N basis using the cathodic-arc-vapor deposition method and the investigation of their physical-mechanical properties is an actual problem of modern materials science.

The purpose of this work is to analyze distribution of elements and contaminations in the films, using the complementary methods of elemental analysis.

## 2. EXPERIMENTAL

The cathodes of high-entropy alloy TiHfVNbZr were prepared by vacuum arc melting in an atmosphere of high purity argon. The melting was performed using a nonconsumable tungsten electrode into a copper water-cooled crucible. Repeating melting for at least 7 times with a cooling rate 50 K/s was carried out to improve chemical homogeneity o f the alloys [8].

The coating was deposited on steel substrate by cathode-vacuum-arc method in a Bulat-6 setup [8] at a substrate bias Us = 100 V and the current arc did not exceed 85 A. The substrate was heated to 400°C before deposition. The deposition rate was set at 1.5 nm/sec.

The elemental composition of the (Ti-Hf-Zr-V-Nb)N coatings and surface morphology were determined using a scanning electron microscope with EDS-analysis JEOL – 7000F (Japan) and JSM-6010LA InTouchScope. To perform the elemental analysis in the depth of the coating, we employed the Rutherford backscattering (RBS) method with He+ ions of 1.7 MeV at normal incidence (the scattering angle was $\theta=170°$). The energy resolution of ion detector was 17 keV. The dose of helium ions was 5 µCi. The standard SIMNRA software [9] was used for processing RBS spectra and obtains profiles of elements distribution in depth of the coating.

One of the effective methods of investigation of depth profile ion sputtering techniques: secondary ion mass spectrometry (SIMS) and glow discharge mass spectrometry (GDMS) [10-14]. For GDMS analysis we used DC 1.8 kV cathode voltage and 0.2 Torr Ar pressure. GDMS analyser SMWJ-01 [15] is equipped with SRS-300 quadrupole mass analyser with 6 mm diameter rods. For SIMS depth profile analysis we used $Ar^+$, 3 keV, 1.5 µA ion beam. SIMS analyser SAJW-05 [16] is equipped with Physical Electronics 06-350E ion gun and QMA-410 Balzers quadrupole mass analyser with 16 mm diameter rods.

## 3. RESULTS AND DISCUSSION

Fig. 1 shows the result of studies of the surface, which were obtained using SEM. As we can see from Fig. 1 the droplet fraction with a size of 10-15 µm have been formed on the surface of nitride coatings during the deposition process. The reflections with the strongest intensity were (111) and (220) XRD lines (see e.g, samples 512, 514, 523). Earlier the works [26-28] have shown that the competition between surface and strain energy determines in general preferred orientation of nitride coatings (OEM model).

* Maryna.Bilokur@gmail.com

**Table 1** – Deposition conditions for multicomponent coatings (Ti-Hf-Zr-V-Nb)N

| № | Us, B | P, Pa | Concentration, % | | | | | |
|---|---|---|---|---|---|---|---|---|
| | | | N | Ti | V | Zr | Nb | Hf |
| 509 | 100 | 3×10-2 | 44.70 | 25.31 | 4.57 | 7.60 | 7.99 | 9.83 |
| 515 | 200 | 3×10-2 | 36.05 | 20.13 | 2.28 | 17.12 | 17.50 | 6.93 |
| 510 | 50 | 2×10-1 | 49.11 | 19.67 | 5.65 | 7.68 | 8.24 | 9.64 |
| 506 | 100 | 2×10-1 | 49.05 | 22.92 | 5.04 | 6.84 | 7.47 | 8.68 |
| 514 | 200 | 2×10-1 | 47.69 | 16.41 | 1.93 | 13.34 | 13.90 | 6.72 |
| 507 | 50 | 5×10-1 | 51.13 | 25.31 | 4.72 | 5.70 | 6.31 | 6.84 |
| 505 | 110 | 5×10-1 | 49.15 | 16.63 | 5.91 | 8.17 | 8.88 | 11.26 |

According to this model, the competing planes in the film with NaCl-type structure are the (200) plane with the lowest surface energy, the (111) plane with the lowest strain energy and the (220) plane with the lowest stopping energy. However, much of studies have showed that there is no universal relation between orientation and intrinsic stress, and the change in the stress state with the increasing coating thickness 21-24].

According to recent works [21, 23-25] the kinetic constraints are assumed to affect the preferential orientation (anisotropy in surface diffusivities, adatom mobilities and collisional cascade effects). On the one hand, the (111) plane is more close-packed of NaCl



**Fig. 1** – The results of XRD diffraction analysis for samples (according to the Table 1)

structure, while the [220] plane is the most open channeling direction. Consequently, the (220) plane have a higher probability of survival than the (111) planes (anisotropy of collision effect). On the other hand, the diffusion of metal adatoms on the (111) surface is less than on the (200) surface, that's why adatoms on (200) planes can be incorporated into the (111) plane. Therefore, the (111) preferred orientation appears. As a result, the preferred orientation of nitride coating develops through a complex interplay between "kinetic" ef-

fects, which associated with the growth process itself.

In the current system, the nitrides of constituting elements (TiN, VN, ZrN, HfN and NbN) represent cubic phase structure NaCl (see table. 2). On this basis, we can make an assumption about the formation of coatings obtained in the single-phase solid solution with an fcc lattice with randomly distributed atoms of the constituent elements. In confirmation of this hypothesis it would be useful to compare values of the diffraction angle responsible for the reflection from the (111) plane and the lattice parameters for binary nitrides and nitride coatings by $M_{HEA}N$ type. As can be seen in Fig. 1 reflex position corresponding to reflection from the (111) plane corresponds to the 35,8°angle, which is approximately equal to the average angle which corresponds to (111) reflex for binary nitrides constituents (see Table. 2). The lattice parameter measured for nitride coating (0.4376 nm) is also slightly different from the lattice of binary nitrides. Thus, the arguments indicate formation of a single phase solid solution with a simple crystal lattice of a nitride-based system Ti-Hf-Zr-V-Nb alloy.

In the same time ion sputtering techniques is mainly used for depth profile analysis [18-20]. In our work we used secondary ion mass spectrometry (SIMS) and glow discharge mass spectrometry (GDMS) for investigation depth profile. Both methods use argon sputtering, however the ionization mechanisms of the sputtered material are different. In SIMS, the ionization occurs at the bombardment surface, and neighboring atoms influence strongly the ionization process due to the so-called matrix effect, the process. In GDMS, ionization occurs mainly above bombardment surface in glow discharge and the matrix effects are negligible. It should be noted that these methods are destructive. Fig. 2 shows the sample after SIMS and GDMS analyses.

Mass spectra registered with GDMS and SIMS are shown in Fig. 3 and raw data of depth profile analysis are shown in Fig. 4.

Sputtering conditions in the two methods differed very much. Sputtering rate in GDMS analysis was 5.7 nm/s, while in SIMS sputtering rate was 0.046 nm/s i.e. 2.8 nm/min. As we can see from Fig. 5 the surface of

**Table 2** – The crystal structure of the constituent elements of the binary nitride (Ti-Hf-Zr-V-Nb) N coatings and the value of the diffraction angle responsible for the reflection from the (111) plane

| Crystal structure | TiN | VN | ZrN | HfN | NbN | (Ti-Hf-Zr-V-Nb)N |
|---|---|---|---|---|---|---|
| | FCC | FCC | FCC | FCC | FCC | FCC |
| 2θ (angle) | 35.30 | 35.5 | 33.89 | 33.6 | 36 | 35.8 |
| Lattice parameter, nm | 0.424 | 0.4132 | 0.458 | 0.452 | 0.442 | 0.4376 |



**Fig. 2** – The sample surface after SIMS and GDMS analyses

nitride coating is covered with a thin oxide film, as detected species are ZrO, NbO, HfO and $ZrO_2$ ions and also contains the high concentration of titanium and vanadium. The presence of uncontrolled impurities (H, C and O) is obviously connected with the residual gases in the working chamber.

Ions currents are shown versus sputtering time in seconds. Raw data of GDMS show strong signal of mass 14 ($N^+$). This signal remains strong after sputtering the interface between nitride and the substrate. So it means that this signal is background affected. Namely in GDMS we detect strong so called plasma noise of mass 14. Also as we can see from Fig. 4 in SIMS tech-nique the ion current decreases with sputtering time, obvious due to the sputtering of surface layer, which include the oxygen. In the other had, we can see the initial rise of ion current in GDMS technique due to the development of direct current glow discharge condition

Basing on the concentration data obtained by EDX technique (N – 44.7%, Ti – 25.31%, V – 4.57%, Zr – 7.60%, Nb – 7.99%, Hf – 9.83%) we perform normalization of the registered ions currents following formula: $I_x / \sum I_x$, where $I_x$ is the normalized ion current of a given component $X$ and $\sum I_x$ is the sum of the normalized ion currents of all registered components. It should be noted that the sensitivity factors used in SIMS differ up to two orders of magnitude and the ratio $I_x / \sum I_x$ represent the relative concentration of elements if we assume equal matrix effect for all elements. In the other hand, the sensitivity of GDMS are close to 1 and the current ratio $I_x / \sum I_x$ also indicate the relative concentration of analyzed elements since no matrix effect are present in this method [6].

Ions currents are shown versus sputtering time in seconds. Raw data of GDMS show strong signal of mass 14 ($N^+$).
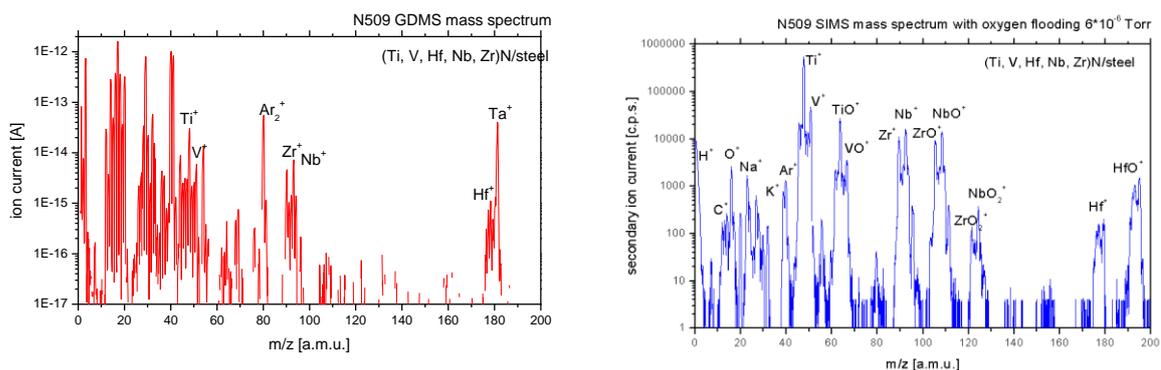


**Fig. 3** – SIMS and GDMS mass spectra for the sample registered in range up to 200 a.m.u.
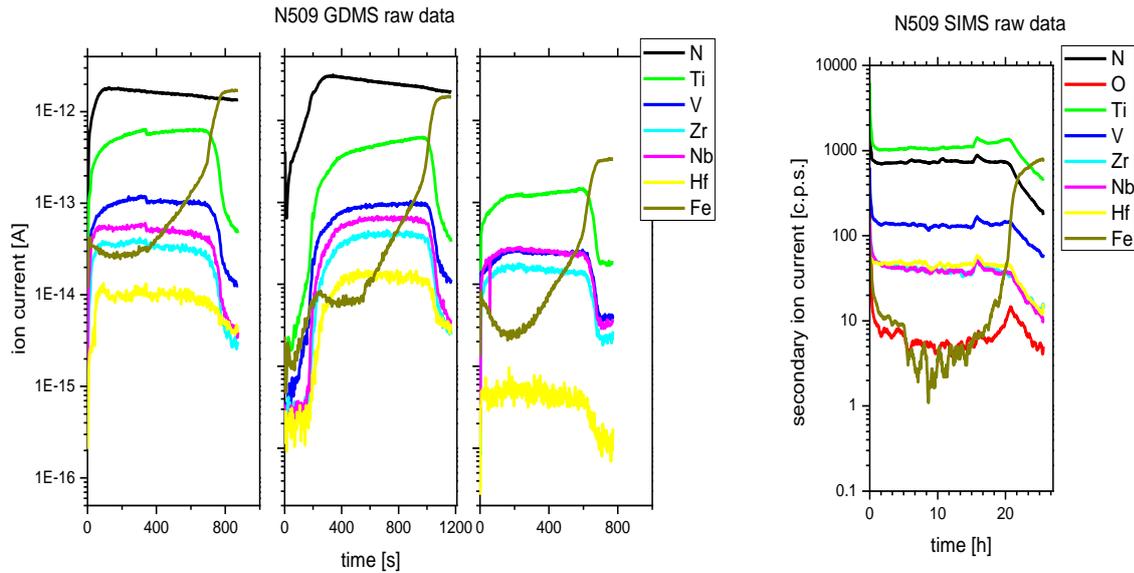
**Fig. 4** – Depth profile analysis. Raw data of GDMS (three analysed spots) and SIMS (one crater)

This signal remains strong after sputtering the interface between nitride and the substrate. So it means that this signal is background affected. Namely in GDMS we detect strong so called plasma noise of mass 14. Also as we can see from Fig. 4 in SIMS technique the ion current decreases with sputtering time, obvious due to the sputtering of surface layer, which include the oxygen. In the other had, we can see the initial rise of ion current in GDMS technique due to the development of direct current glow discharge condition.

Basing on the concentration data obtained by EDX technique (N – 44.7%, Ti – 25.31%, V – 4.57%, Zr – 7.60%, Nb – 7.99%, Hf – 9.83%) we perform normaliza-tion of the registered ions currents following formula: $I_x/\sum I_x$, where $I_x$ is the normalized ion current of a given component $X$ and $\sum I_x$ is the sum of the normalized ion currents of all registered components. It should be noted that the sensitivity factors used in SIMS differ up to two orders of magnitude and the ratio $I_x/\sum I_x$ represent the relative concentration of elements if we assume equal matrix effect for all elements. In the other hand, the sensitivity of GDMS are close to 1 and the current ratio $I_x/\sum I_x$ also indicate the relative concentration of analyzed elements since no matrix effect are present in this method [6].



**Fig. 5** – Depth profile analysis of the sample (including nitrogen) – left GDMS and right SIMS

Both methods show element profiles, as we can see the result show the same compositional changes in the analyzed sample. The Hf, Zr, Nb and V profiles are similar in SIMS and GDMS methods, while the titanium profiles are different in two methods. Both techniques show that distribution of metal components across the layer is stable, however titanium concentration slightly increases towards the interface, while the concentrations of Nb, Hf, Zr slightly decrease.

## 4. CONCLUSIONS

New nitride coating based on the TiHfVNbZr high-entropy alloy has been fabricated. The coating exhibits a single cubic (NA-Cl) nitride phase. By combining the results of the RBS and the results obtained with ion sputtering technique (SIMS and GDMS) methods we received a more realistic picture of the distribution of constituent elements over the depth of the layer. Both analytical methods, SIMS and GDMS give same results. However, the slight deviation in case of nitrogen direction connected with the strong influence of plasma noise.

### REFERENCES

1. J.W. Yeh, Yu.L. Chen, S.J. Lin, S.K. Chen, *Mat. Sci. For.* **560**, 1 (2007).
2. Y. Zhang, T.T. Zuo, Z. Tang, M.C. Gao, K.A. Dahmen, P.K. Liaw, Z.P. Lu, *Prog. Mater. Sci.* **61**, 1 (2014).
3. A.D. Pogrebnjak, *J. Nanomater.* **2013,** 1 (2013).
4. T.K. Chen, M.S. Wang, T.T. Shun, J.W. Yeh, *Surf. Coat. Technol.* **200**, 1361 (2005).
5. A.D. Pogrebnjak, *Mater. Sci. Appl.* **4**, 14 (2013).
6. P. Konarski, K. Kaczorek, D. Kaliński, M. Chmielewski, K. Pietrzak, M. Barlak, *Surf. Interf. Anal.* **45**, 494 (2013).
7. P. Konarski, K. Kaczorek, J. Senkara, *Surf. Interf. Anal.* **43**, 217 (2011).
8. O.V. Sobol', A.A. Andreev, V.F. Gorban, N. Krapivka, V.A. Pole, I.V. Serdyuk, V.E. Filchikov, *Tech. Phys. Lett.* **38**, 616 (2012) [in Russian].
9. Simnra.com
10. V.I. Lavrentiev, A.D. Pogrebnjak, *Surf. Coat. Technol.* **99**, 24 (1998).
11. A.D. Pogrebnjak, A.P. Shpak, V.M. Beresnev, D.A. Kolesnikov, Yu.A. Kunitskii, O.V. Sobol, V.V. Uglov, F.F. Komarov, A.P. Shypylenko, N.A. Makhmudov, A.A. Demyanenko, V.S. Baidak, V.V. Grudnitski, *J. Nanosci. Nanotech.* **12**, 9213 (2012).
12. A.D. Pogrebnjak, A.P. Shpak, N.A. Azarenkov, V.M. Beresnev, *Phys. Usp.* **52**, 29 (2009) [in Russian].
13. A.D. Pogrebnjak, V.N. Borisyuk, A.A. Bagdasaryan, *Cond. Mat. Phys.* **16**, 1 (2013).
14. A.D. Pogrebnjak, Yu.A. Kravchenko, S.B. Kislitsyn, Sh.M. Ruzimov, F. Noli, P. Misaelides, A. Hatzidimitriou, *Surf. Coat. Technol.* **201**, 2621 (2006).
15. P. Konarski, K. Kaczorek, M. Ćwil, J. Marks, *Vacuum* **81**, 1323 (2007).
16. P. Konarski, A. Mierzejewska, *Appl. Surf. Sci.* **203**, 354 (2003).
17. R.L. Boxman, V.N. Zhitomirsky, *Rev. Sci. Instr.* **77**, 021101 (2006).
18. V. Ivashchenko, S. Veprek, A.D. Pogrebnjak, B. Postolniy, *Sci. Technol. Adv. Mater.* **15**, 025007 (2014).
19. O.V. Sobol, A.D. Pogrebnyak, V.M. Beresnev, *Phys. Met. Metall.* **112**, 188 (2011) [in Russian].
20. A.D. Pogrebnjak, A.G. Ponomarev, A.P. Shpak, Yu.A. Kunitskii, *Phys. Usp.* **55**, 270 (2012) [in Russian].
21. G. Abadias, *Surf. Coat. Technol.* **202**, 2223 (2008).
22. I. Petrov, L. Hultman, J.E. Sundgen, J.E. Green, *J. Vac. Sci. Technol. A* **10**, 265 (1992).
23. P. Patsalas, C. Gravalidis, S. Logothetidis, *J. Appl. Phys.* **96**, 6234 (2004).
24. D. Gall, S. Kodambaka, M.A. Wall, I. Petrov, J.E. Greene, *J. Appl. Phys.* **93**, 9086 (2003).
25. L. Hultman, J.E. Sundgren, J.E. Greene, D.B. Bergstrom, I. Petrov, *J. Appl. Phys.* **78**, 5395 (1995).
26. R.L. Boxman, V.N. Zhitomirsky, *Rev. Sci. Instrum.* **77**, 021101 (2006).
27. J. Pelleg, L.Z. Zevin, S. Lungo, *Thin Solid Films* **197**, 117 (1991).
28. J.H. Je, D.Y. Noh, H.K. Kim, K.S. Liang, *J. Appl. Phys.* **81**, 6126 (1997).